*Bull. Mater. Sci.* (2023)46:94
https://doi.org/10.1007/s12034-023-02929-z



# Factors affecting photocatalytic degradation of methyl red by $MoS_2$ nanostructures prepared by hydrothermal technique

**ANJALI RANI[1], KULVINDER SINGH[2], ARUN SINGH PATEL[3] and PRIANKA SHARMA[1,*]**

[1]Department of Physics, School of Basic and Applied Sciences, Maharaja Agrasen University, Solan 174103, India
[2]Department of Chemistry, DAV College, Chandigarh 160011, India
[3]Department of Physics, Hindu College, New Delhi 110007, India
*Author for correspondence (drpriankasharma@gmail.com)

MS received 31 July 2022; accepted 28 December 2022

**Abstract.** In this study, we have synthesized $MoS_2$ nanostructures (NSs) through a simple and facile hydrothermal method and studied various factors affecting the degradation of organic azo dye methyl red (MR) under the illumination of visible light. The as-synthesized photo-catalyst has been characterized by powder X-ray diffraction, Raman spectroscopy and transmission electron microscopy to confirm its structure and surface morphology. The results reveal that the prepared $MoS_2$ NSs have 2H crystal phase. The peak frequency difference of $\sim 25\ cm^{-1}$ exhibits preparation of 5–6 layers of $MoS_2$ NSs. Ultraviolet–visible spectroscopy has been utilized to study the change in percentage degradation of the dye with variation in dosages of photocatalyst, dye concentration and variation in pH of the dye. $MoS_2$ NSs show the best adsorption of 80.35% at low pH of 4.24 with 14 mg of catalyst dosage and 50 ppm of dye concentration in 6 h of irradiation time.

**Keywords.** Photocatalysis; hydrothermal method; pH; concentration of photocatalyst; pollutant concentration.

## 1. Introduction

In recent era, with growth in industrialization, wastewater and effluent from industries have been the major sources of water pollution. Textile, leather manufacturing, furniture and plastic industries, all make excessive use of synthetic dyes. These dyes when released as effluent from industries, mix with water bodies to increase the toxicity of water and are resistant to biodegradation. Dyes absorb oxygen dissolved in water bodies and undergo various biological and chemical reactions like hydrolysis and oxidation, which poses threat to the aquatic life and cause a major role in environmental degradation. Thus, the treatment of wastewater from industries is one of the major concerns of environmentalists. Different conventional techniques like ultrafiltration, activated carbon adsorption, ion exchange on synthetic adsorbent resins and coagulation by chemical agents have been commonly utilized for dye degradation [1–5]. However, the incapability of these conventional techniques of dye degradation has motivated the search for advanced oxidation processes for the complete removal of toxic dyes from wastewater and effluents released from industries. Moreover, the process should be less time-consuming and cost-effective. In this context, photocatalysis proves to be an effective technique, which leads to quick formation of hydroxyl radicals that has the capability of oxidizing wide range of pollutants present in water without any preference of selectivity [6, 7]. Among many photocatalysis systems, semiconductor-mediated photocatalysis have been investigated widely for complete mineralization of organic pollutants present in water [8–14]. $TiO_2$ and ZnO nanoparticles are popular choice for photocatalytic degradation of organic dyes. Both have wide bandgap 3–3.25 eV ($TiO_2$) and 3.25eV (ZnO), and undergo identical photocatalytical mechanism [15]. Other wide bandgap semiconductor-based photocatalysts CdS, $SnO_2$ and ZnS have attracted enormous attention due to their antibacterial applications as well as high sensitivity [16–19]. In addition, photocatalysis is initiated by photoexcitation of charges, resulting in separation of electron–hole pairs and interfacial charge transfer. The excitation of electrons and holes leads to imbalance of charge transfer, which tend to the recombination of electron–hole pairs, thereby reducing the overall efficiency of the photocatalysis activity. So fast recombination of electron–hole pairs in semiconductors and their responsitivity towards UV excitation restrict their application as good photocatalyst [20, 21]. Thus, alternative approaches have been looked upon to overcome the limitations of semiconductor photocatalysts. Other alternatives like doping of semiconductor photocatalyst with non-metals like C, B, N, F and S show improved degradation capabilities [22, 23]. However synthesizing N-doped $TiO_2$ reduces the bandgap from 3.25 to 2.5 eV and make it active for visible-light photocatalysis

Published online: 04 May 2023

[24, 25]. Similarly, doping of ZnO with Ce also shows significant enhancement in the degradation efficiency [26].

In this search, transition metal dichalcogenide $MoS_2$ proves to be a promising candidate for photocatalysis of dyes [27–29]. $MoS_2$ exhibits indirect bandgap of 1.2 eV as bulk, which can be tuned to direct bandgap of 1.97 eV while moving towards few to single-layered system [30]. Combining transition metal dichalcogenide with semiconductors like $TiO_2$ and ZnO nanoparticles showed improved results. Zhang *et al* [31] and Chen *et al* [32] have fabricated $TiO_2$/$MoS_2$ for photocatalytic applications. Benavente *et al* [33] have reported synthesis of heterostructured ZnO/$MoS_2$ layered hybrid of nanostructures (NSs) for increased visible photocatalyst activity, but not much work has been done on the $SnO_2$/$MoS_2$ composite for photocatalytic activity. Au-$MoS_2$ and $SnO_2$-$MoS_2$ NS showed enhanced degradation efficiency of methyl red (MR) up to 96.7 and 94%, respectively [13, 14]. Its tuneable bandgap compresses the electron–hole recombination rates thereby giving $MoS_2$ a unique property of getting self-excited under visible as well as UV light irradiation. Since, the phenomenon of photocatalysis include charge transfers between surface of the catalyst and the dye, the efficiency of photocatalysis kinetics and its mechanism can be improved by modifications in their surface structure and properties. Compact degree of $MoS_2$ structure increases the surface area for charge carrier mobility, leading to strong adsorption of dye molecule on the $MoS_2$ catalyst surface. Since surface structure of the catalyst greatly influences the charge transfer processes responsible for photocatalytic activity, the preparation of $MoS_2$ with specific morphology has attracted lot of interest [34]. Ntakadzeni *et al* [35] have fabricated PEGylated $MoS_2$ nanosheets hydrothermally for photodegradation of organic dyes. Recently, Luo *et al* [34] have studied hydrothermal synthesis of $MoS_2$ with controllable morphologies and its adsorption properties for bisphenol A. Ho *et al* [36] have fabricated $MoS_2$ nanoclusters by an *in-situ* photoreduction deposition method to evaluate photocatalysis activity. From all these works, it can be estimated that surface morphologies play an important role in the photocatalytic activity of different dyes. Besides there are other factors also responsible for affecting the surface characteristics. Reza *et al* [37] reviewed various factors affecting the photocatalytic degradation of dyes. Generally, pH of the dye is an important factor that affects the degradation of dye. Any change in pH can alter the surface characteristics and size of the agglomerated NSs upon which depends the adsorbability of dye molecules on the surface of the NSs and generation of hydroxyl radicals [38]. Thus, many attempts have been made to control the surface properties of the catalyst to enhance the photocatalytic efficiency. This work is preliminary stage for optimizing the parameters for efficient photocatalytic degradation of organic dyes. In the present work, we have prepared layered $MoS_2$ NSs by hydrothermal technique. These $MoS_2$ NSs have been utilized to study the photocatalytic activity of the organic dye MR. The study has been focussed towards investigating the factors like pH of the dye, concentration of the dye and dosage of the catalyst responsible for controlling the efficiency of degradation of the dye. With these optimizing parameters, this work has been further extended to investigate the photocatalytic degradation of organic dyes by $MoS_2$ nanosheets synthesized by different routes [39].

## 2. Experimental

*Materials:* All the chemical reagents were of analytical grade and used without further purification. Ammonium molybdate tetrahydrate [$(NH_4)_6Mo_7O_{24}{\cdot}4H_2O$] and thiourea [$CH_4N_2S$] were purchased from Sigma Aldrich and Nice, respectively, and methyl red from Molychem. All the solutions were prepared in deionized water.

### 2.1 *Synthesis of $MoS_2$ NSs*

$MoS_2$ NSs were synthesized via conventional hydrothermal route using starting precursors: ammonium molybdate tetrahydrate as a source of molybdenum and thiourea as a source of sulphide ions. Briefly, 0.1 M solution of ammonium molybdate tetrahydrate and 0.5 M solution of thiourea were separately prepared in 40 ml of deionized water, mixed and sonicated for 30 min. After sonication, the solution was transferred into a 100 ml Teflon-lined stainless steel autoclave and reaction was carried out in muffle furnace for 15 h at 160°C. After natural cooling of the furnace, the resulting dark brown precipitates were obtained through filtration. The precipitates were further washed many times with deionized water and absolute ethanol to remove any traces of residual ions. The final product was then dried at 60°C for 7 h.

### 2.2 *Photocatalytic activity of $MoS_2$ NSs*

Hydrothermally synthesized $MoS_2$ NSs were tested for degradation of methyl red (MR) dye under visible-light irradiation. In particular, 50 ml (100 ppm) stock solution of MR with neutral pH (7) prepared in distilled water was stirred in dark in order to accomplish adsorption and desorption. A quantity of 0.02 g of catalyst was then added and continuously stirred and dispersion of $MoS_2$ NSs remained stable over time. For exploring the effect of various factors on the degradation of the dye; different catalyst dosages (0.012, 0.014, 0.016, 0.018 and 0.02 g), dye concentrations (25, 50, 75 and 100 ppm) and variation in pH (2.24, 4.24, 6.24, 8.24 and 10.24) were taken in dark. The samples were irradiated under white light (85 Watt CFL) for 6 h. During the photocatalytic process, starting from 0 min after every 30 min time duration, sample was taken out and centrifuged for 10 min at 4000 rpm. Then these samples were further

characterized with UV–visible spectrophotometer for measuring the removal percentage degradation of the dye. The overall preparation method is shown in figure 1.

## 3. Characterization techniques

Panalytical's X'Pert Pro X-ray diffractometer using Cu-Kα radiation ($\lambda = 1.5418$Å) and scanning range from 10° to 70° was used to characterize the structural properties of the $MoS_2$ NSs. Transmission electron microscope JEOL 2100F operated at 200 kV was used to study the surface morphology of the samples. Intra-layer bonding and lattice vibrations were confirmed by Raman spectra of the $MoS_2$ NSs characterized using 532 nm laser source in confocal Raman spectrometer (WITec, ALPH300 RA). Photocatalytic activity of the $MoS_2$ NSs was studied using UV–visible spectroscopy (Labtronics, LT-2700, India).

## 4. Results and discussions

### 4.1 *Structural investigations*

Figure 2a shows the X-ray diffraction patterns of $MoS_2$ NSs synthesized hydrothermally at 160°C for 15 h. Diffraction peaks of $MoS_2$ at $2\theta$ are observed at 14.85, 28.13, 32.89, 33.78, 36.19, 39.82, 44.33, 49.97, 56.19, 58.44, 60.70 and 62.96, which arises from crystal planes of (002), (004), (100), (101), (102), (103), (006), (105), (106), (110), (008) and (107) and matches well with the JCPDS no. 37-1492, respectively [40]. The (002) diffraction peak shows highest diffraction intensity attributing to the presence of randomly stacked few layers of $MoS_2$. No other extra diffraction peaks are observed, which ensure the presence of no impurities in the samples. Therefore, it can be concluded that the pure 2H-$MoS_2$ sample, with better crystallinity, was prepared at 160°C-15 h. Figure 2b represents the transmission electron microscope image of $MoS_2$, which reveals agglomeration of many spherical-like aggregated particles. Coagulation into sphere is due to the precursor used and the hydrothermal reaction condition. During the reaction, ammonium molybdate tetrahydrate releases $MoO^{4-}$ ions, whereas thiourea releases sulphide ions. These $MoO^{4-}$ ions further reacts with the sulphide ions, which promote the self-assembly of a sphere-like morphology.

### 4.2 *Optical investigations*

Figure 3a and b shows the Raman spectroscopy and the UV–visible absorption spectroscopy used to illustrate the as-synthesized $MoS_2$ nanosheets. Raman spectroscopy was used to study the vibrational modes as well as number of layers of $MoS_2$ NSs. Generally, $MoS_2$ has two typical Raman peaks, one is $E^1_{2g}$(in-plane mode) resulting by the opposite vibration of Mo with respect to the two S atoms and another is $A_{1g}$ (out-of-plane mode) attributed by the vibration of only S atoms in opposite direction. From figure 3a, we observe that the $MoS_2$ exhibits $E^1_{2g}$ and $A_{1g}$ modes at 381.04 and 406.09 $cm^{-1}$ with sharp intensity which indicates that the material is highly crystalline at 160°C. The difference between these two modes i.e., $E^1_{2g}$

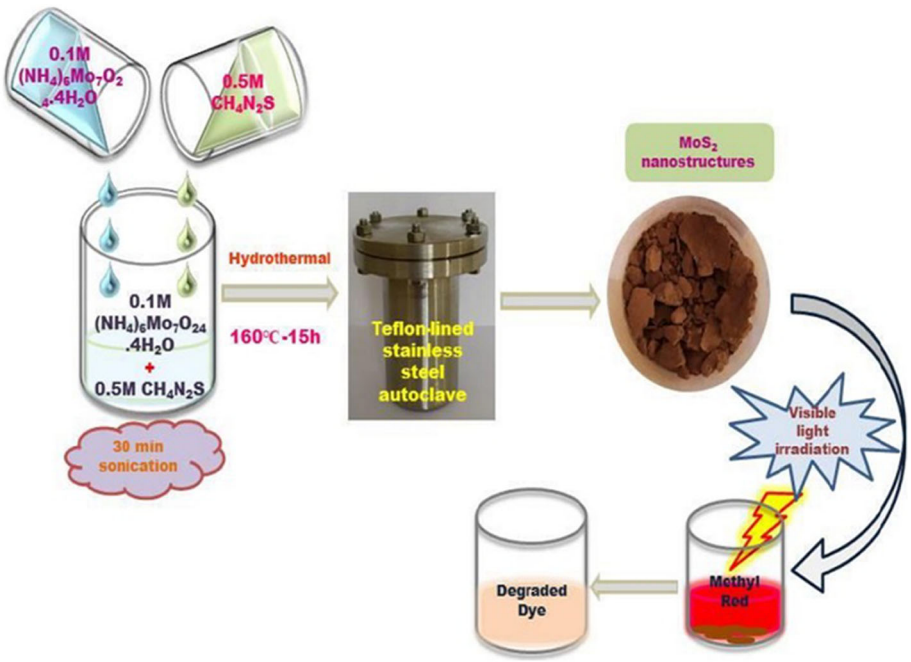


**Figure 1.** Schematic diagram for hydrothermal synthesis of $MoS_2$ and assisted photodegradation of methyl red.

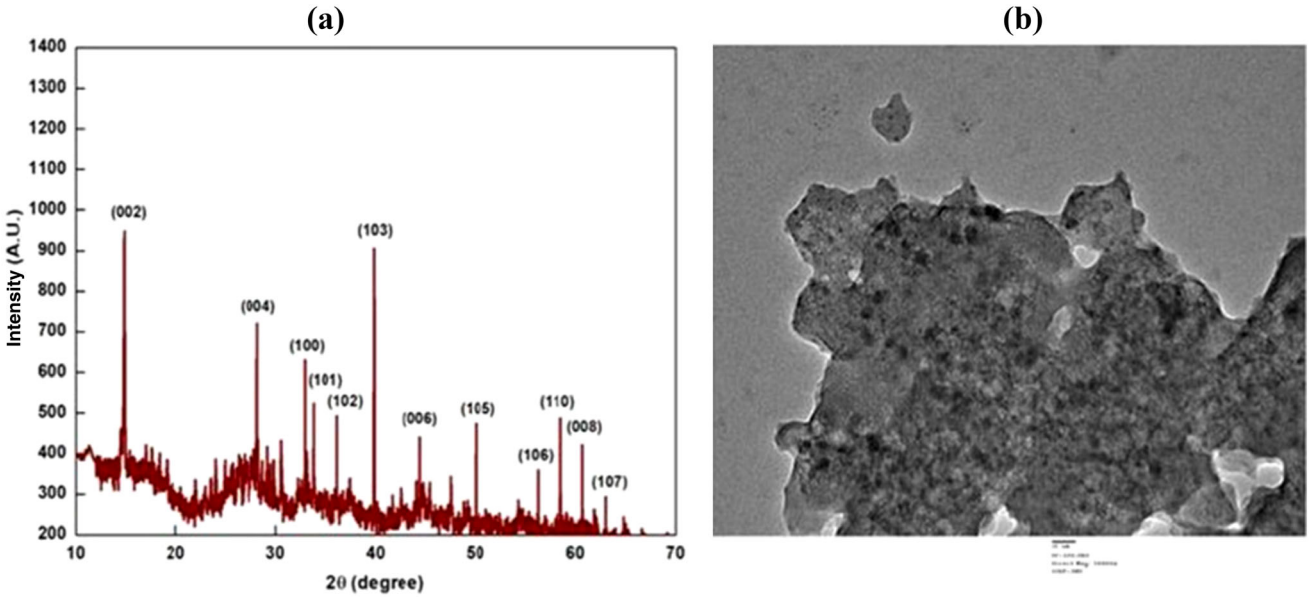


**Figure 2.** (**a** and **b**) XRD pattern and transmission electron microscopy (TEM) images of the hydrothermally prepared $MoS_2$ NSs at 160°C for 15 h.

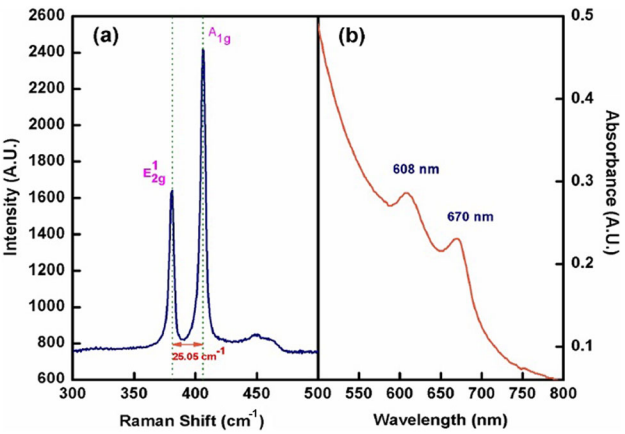


**Figure 3.** (**a** and **b**) Raman spectra and UV–visible spectra of the $MoS_2$ NSs prepared hydrothermally at 160°C for 15 h.

and $A_{1g}$ modes (Δ) come out to be ~25 cm$^{-1}$, which corresponds to 5–6 layers of $MoS_2$ and matches well with the reported work [41]. From figure 3b, it is clear that the prepared $MoS_2$ exhibits two peaks at around 608 and 670 nm corresponding to the excitonic transitions that occur due to spin-orbit splitting [41], which are related to the bandgap of the material. The result reveals the ability of the $MoS_2$ to absorb light in both UV and visible-light range of the spectrum, which indicates its use as a photocatalyst for the degradation of the pollutants.

### 4.3 *Visible-light reactive photocatalytic activity*

Photodegradation efficiency of $MoS_2$ NSs was investigated on MR organic dye. Intensity of the characteristic absorption peak of MR at 522 nm using the UV–Visible spectrophotometer was used to track its concentration in the solution. There was no noticeable change in the colour of untreated MR dye and treated MR dye solution in dark as compared to irradiated under white light for the same amount of time (6 h).

*4.3a Effect of concentration of catalyst*: Catalyst dosage greatly influences the rate of degradation of the dye. It has been observed by many groups that rate of degradation initially increases with increase in catalyst dosages, as shown in figure 4a. However, increasing the dosage levels above a certain limit, degradation rate remain constant or decreases [10]. According to Beer-Lambert's law, percentage degradation efficiency is calculated on the basis of proportionality of concentration of dye to its absorbance, given by equation (1) [39].

$$R = \frac{C_o - C}{C_o} \times 100\% = \frac{A_o - A}{A_o} \times 100\% \quad (1)$$

where $C_o$, $C$ are the concentrations and $A_o$, $A$ are the absorbance of dye at initial time (0) and after '$t$' hour, respectively.

To examine the kinetic studies on the adsorption of MR by prepared $MoS_2$ NSs, normalized absorption $C/C_o$ (where $C_o$ = concentration at time $t = 0$, $C$ = concentration at time $t$) decays exponentially with time given by equation (2), which exhibit that the degradation is a pseudo-first-order reaction as observed in figure 4b.

$$\ln \frac{C}{C_o} = kT \quad (2)$$

In the present work, different dosages of $MoS_2$ (0.012, 0.014, 0.016, 0.018 and 0.02 g) has been used to investigate

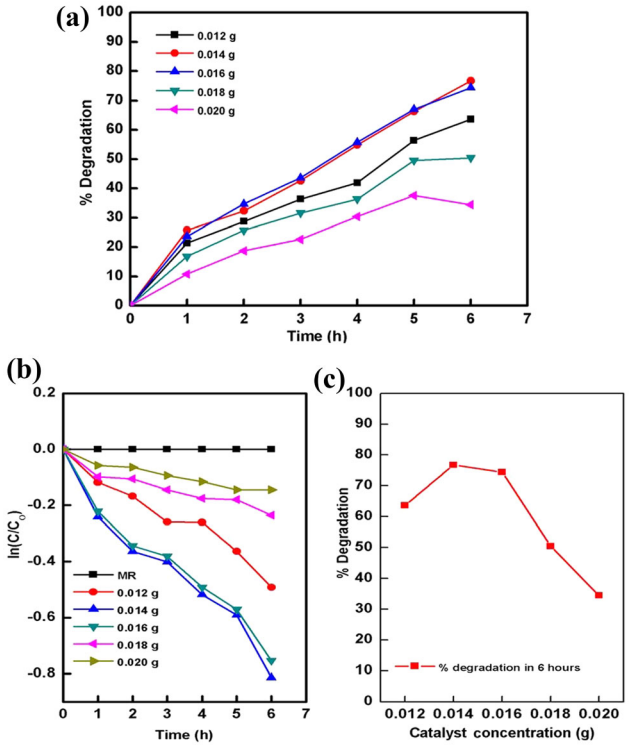


**Figure 4.** (**a**) Percentage degradation and (**b**) $\ln C/C_O$ *vs.* time of MR with different dosages of $MoS_2$ (12–20 mg with an increase of 2 mg) irradiated under visible light for 6 h. (**c**) Percentage degradation of MR after 6 h at different $MoS_2$ concentrations.

the effect of dosage of photocatalyst on the percentage degradation of MR. From figure 4, we observe that the rate of degradation varies directly with the dosage of $MoS_2$. Percentage degradation of the dye increases as the dosage of $MoS_2$ increases from 0.012 to 0.014 g. Correspondingly, the rate constant also varies from 0.2371 to 0.4184 $h^{-1}$, respectively. This indicates heterogeneous nature of $MoS_2$. However, for the concentration of 0.016 g of $MoS_2$, the degradation rate constant is 0.3946 $h^{-1}$. With further increase in dosage of $MoS_2$, percentage degradation of the dye and the rate constant values decrease exhibiting a negative effect of increase in dosage of the catalyst after a certain limit. Figure 4b and c exhibits variation in ln $C/C_o$ *vs.* time and percentage degradation of MR with different $MoS_2$ dosages (0.012–0.020 g with the increase of 0.002 g) after 6 h, respectively. Table 1 shows variation in the rate constant values for different dosages of $MoS_2$. The reason behind degradation of dye can be explained on the basis of available active sites for photocatalysis. As concentration of catalyst ($MoS_2$) increases, available active sites on the surface of the catalyst increases [39]. However, at the same time, due to high concentration of the catalyst, turbidity of the suspension increases which reduces the photo-activated volume of suspension. This diminishes the penetration of light to the active sites of the catalyst for photodegradation. Another possible reason might be agglomeration of $MoS_2$ particles in the dye solution at higher concentration. Agglomeration of the catalyst leads to collision of the activated molecules with the ground-state molecules. This decreases the available sites for absorption of photon and the dye on the catalyst surface, thereby suppressing the catalytic activity of $MoS_2$. In the present work, an optimum dosage of 0.014 g of $MoS_2$ showed better degradation of the dye with rate constants 0.4184 $h^{-1}$.

*4.3b Effect of dye concentration:* Initial concentration of dye also plays a major role in the study of photocatalysis of the dye. Similar to the effect of concentration of catalyst, in the present work, the rate of degradation increases for an increase in the concentration of dye up to a certain limit, thereafter a declining trend has been observed for a higher concentration of dye. Figure 5a exhibits percentage degradation of MR at different dye concentrations (25, 50, 75 and 100 ppm) with optimized 0.014 g of $MoS_2$. It has been observed that for lower concentrations of dye 25 and 50 ppm, percentage degradation is 70.58 and 76.74%, respectively. However, as the dye concentration increases, sharp decrease in the degradation curve has been observed for 75 ppm (52.35% degradation) and 100 ppm (44.68% degradation). Figure 5b and c shows $\ln C/C_O$ *vs.* time and percentage degradation of MR after 6 h at different dye concentrations (25, 50, 75 and 100 ppm) by 0.014 g of $MoS_2$, respectively. Variation in rate constant values for different concentrations of MR is presented in table 2. A similar trend in degradation of organic dyes have been observed by many groups. This might be due to the reason that the photocatalytic degradation depends on the presence of hydroxyl radical $(OH^{\bullet})$ on the surface of catalyst and probable reaction of this hydroxyl radical with the dye molecule. At low concentration of dye, more photons are absorbed by the catalyst, which increases the formation of these $OH^{\bullet}$ radicals. At higher concentration of dye, the active sites of the catalyst get covered by the increased number of dye ions. As a result, lesser number of $OH^{\bullet}$ are formed on the catalyst surface, which reduces the oxidation of the dye molecules with these $(OH^{\bullet})$ radicals. Another possible reasoning behind this effect might be that at higher concentration of dye, most of the light is absorbed by the dye molecule instead of the catalyst NSs. This reduces the formation of hydroxyl radical $(OH^{\bullet})$ and superoxide radical anion $\left(O_2^{\bullet-}\right)$, thereby reducing the efficiency of the photodegradation reaction [42, 43]. Thus it was concluded that an optimum dosages of 50 ppm of dye concentration with 14 mg of catalyst ($MoS_2$) shows improved degradation of the dye.

*4.3c Effect of pH of dye*: Since effluent water from textile industries contaminated with different dyes is released at different pH, it is also important to investigate the effect of pH on degradation of dyes. In order to study the effect of pH on the degradation efficiency, the present work has been carried out at various pH ranging from 2.42, 4.24, 6.24, 8.24 and 10.42 for constant dye concentration of 50 ppm/50 ml

**Table 1.** Variation in rate constant values for different dosages of $MoS_2$ (0.012, 0.014, 0.016, 0.018 and 0.020 g).

| Catalyst concentration (g) | Percentage degradation of MR with visible-light irradiation time | | | | | | Rate constants ($h^{-1}$) |
|---|---|---|---|---|---|---|---|
| | 1 h | 2 h | 3 h | 4 h | 5 h | 6 h | |
| 0.012 | 21.34 | 28.76 | 36.35 | 41.87 | 56.36 | 63.58 | 0.2371 |
| 0.014 | 25.75 | 32.31 | 42.63 | 54.89 | 66.23 | 76.74 | 0.4184 |
| 0.016 | 23.68 | 34.67 | 43.57 | 55.75 | 67.00 | 74.43 | 0.3946 |
| 0.018 | 16.78 | 25.67 | 31.57 | 36.35 | 49.53 | 50.43 | 0.1340 |
| 0.020 | 10.78 | 18.67 | 22.57 | 30.35 | 37.53 | 34.43 | 0.0884 |

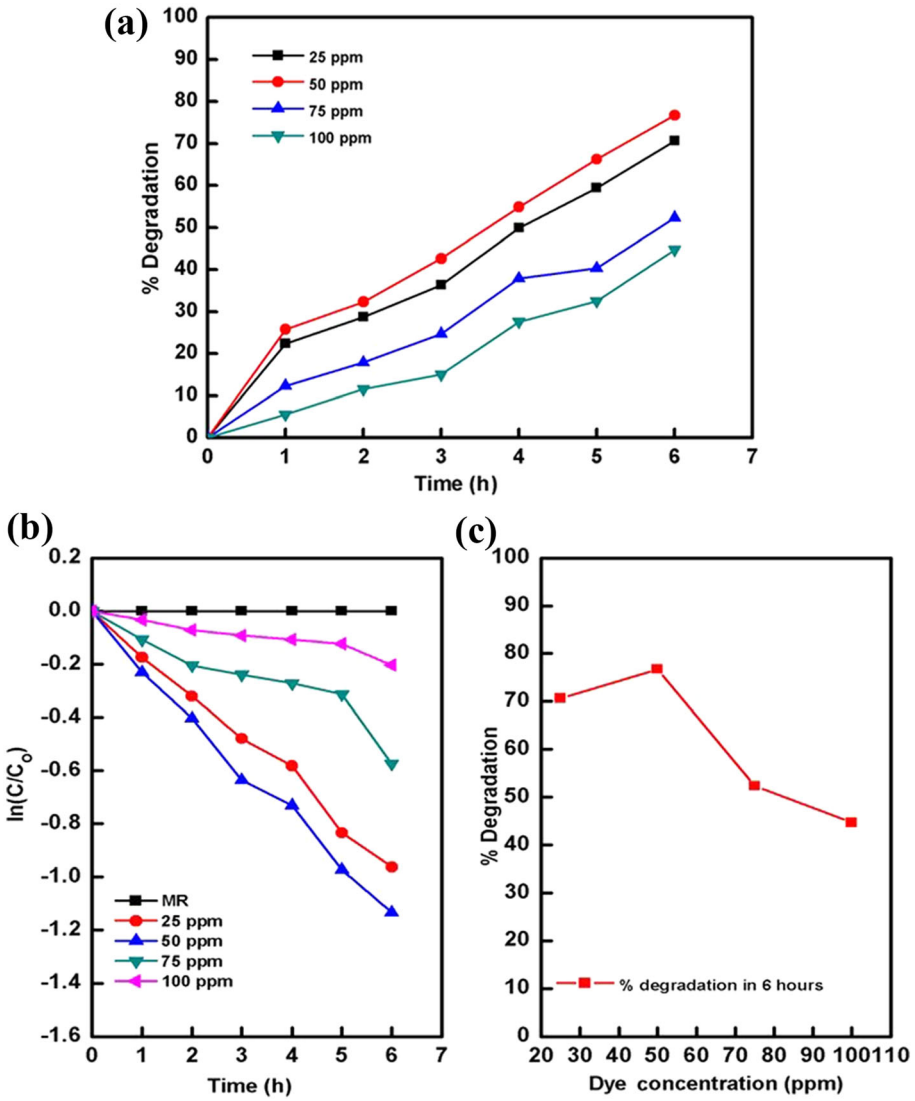


**Figure 5.** (**a**) Percentage degradation and (**b**) $\ln C/C_O$ *vs.* time of MR in 6 h at different dye concentrations (25, 50, 75 and 100 ppm) with optimized value (0.014 g) of $MoS_2$ catalyst. (**c**) Percentage degradation of MR after 6 h at different dye concentrations by 0.014 g of $MoS_2$ as catalyst.

and 0.014 g of catalyst dosage. From figure 6a, it has been observed that percentage degradation increases as we go towards low pH in the acidic region whereas as the pH increases, the degradation percentage decreases towards alkaline region. Figure 6b and c shows $\ln C/C_O$ *vs.* time and percentage degradation of MR after 6 h at different pH

**Table 2.** Variation in rate constant values for different concentrations of MR (25, 50, 75 and 100 ppm).

| Dye concentration (ppm) | Percentage degradation of MR with visible-light irradiation time | | | | | | Rate constants ($h^{-1}$) |
|---|---|---|---|---|---|---|---|
| | 1 h | 2 h | 3 h | 4 h | 5 h | 6 h | |
| 25 | 22.34 | 28.76 | 36.35 | 49.87 | 59.36 | 70.58 | 0.4789 |
| 50 | 25.75 | 32.31 | 42.63 | 54.89 | 66.23 | 76.74 | 0.4252 |
| 75 | 12.35 | 17.88 | 24.68 | 37.88 | 40.33 | 52.34 | 0.2446 |
| 100 | 5.54 | 11.5 | 15.01 | 27.53 | 32.53 | 44.68 | 0.0859 |

values by 14 mg $MoS_2$ (catalyst) with 50 ppm concentration, respectively. Variation in rate constant values for different pH of MR is presented in table 3. Maximum and optimum degradation was observed for acidic pH-4.24 (80.35%). Similar photocatalytic efficiency behaviour has been reported for ZnO and $TiO_2$ for degradation of azo dyes [44, 45]. It is quite difficult to explain the effect of different pH on the efficiency of degradation due to multiple on going mechanisms for the photocatalytic process. Three reaction mechanisms basically contribute to degradation of dye, namely, direct reduction by the electron in the conducting band, direct oxidation by the positive holes and

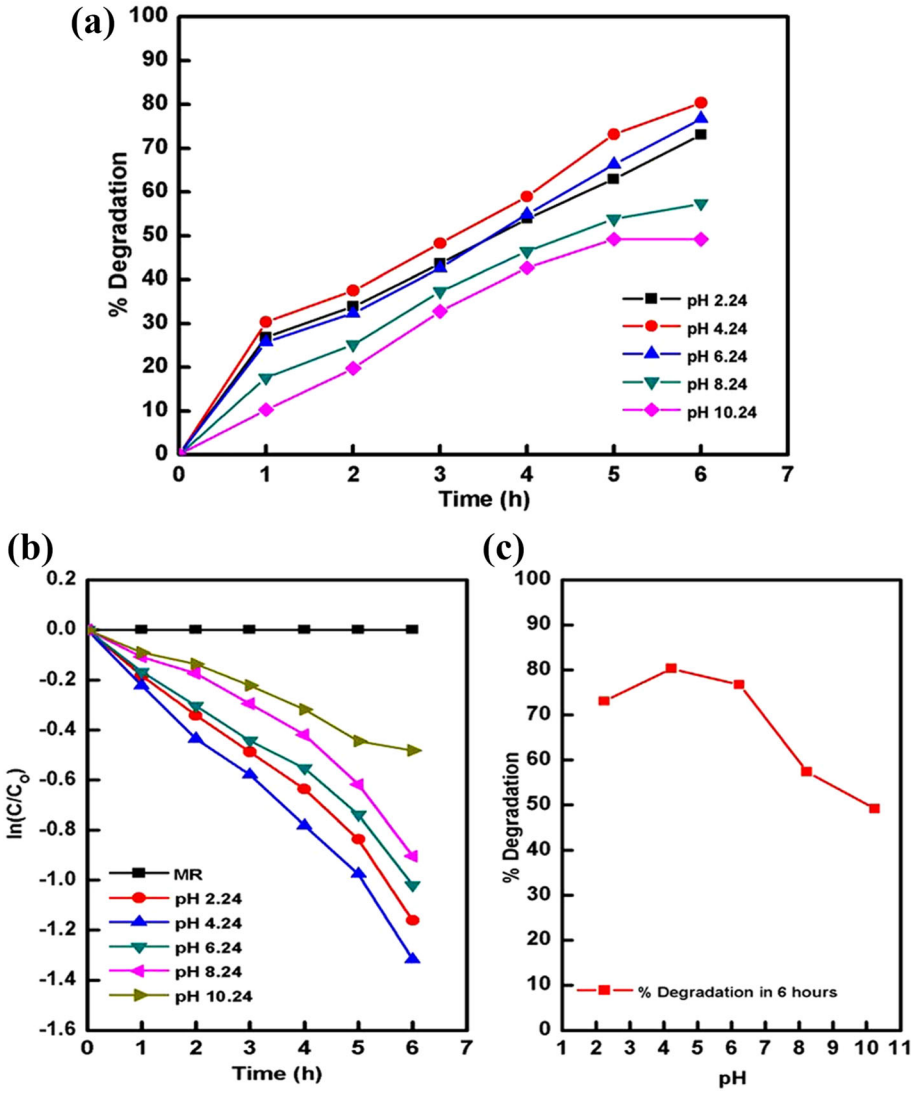


**Figure 6.** (**a**) Percentage degradation and (**b**) $\ln C/C_O$ *vs.* time of MR (50 ppm) by 0.014 g of $MoS_2$ catalyst at different pH values (2.24, 4.24, 6.24, 8.24 and 10.24). (**c**) Percentage degradation of MR (50 ppm) after 6 h at different pH values by 0.014 g of $MoS_2$ as catalyst.

**Table 3.** Variation in rate constant values for different pH values of MR (2.24, 4.24, 6.24, 8.24 and 10.24).

| | Percentage degradation of MR with visible-light irradiation time | | | | | | |
|---|---|---|---|---|---|---|---|
| pH (Dye) | 1 h | 2 h | 3 h | 4 h | 5 h | 6 h | Rate constants ($h^{-1}$) |
| 2.24 | 26.82 | 33.86 | 43.67 | 53.88 | 62.88 | 73.04 | 0.3552 |
| 4.24 | 30.35 | 37.50 | 48.21 | 58.92 | 73.21 | 80.35 | 0.4278 |
| 6.24 | 25.75 | 32.31 | 42.63 | 54.89 | 66.23 | 76.74 | 0.3149 |
| 8.24 | 17.57 | 25.11 | 37.35 | 46.45 | 53.79 | 57.36 | 0.3597 |
| 2.24 | 10.25 | 19.78 | 32.76 | 42.68 | 49.23 | 49.14 | 0.2288 |

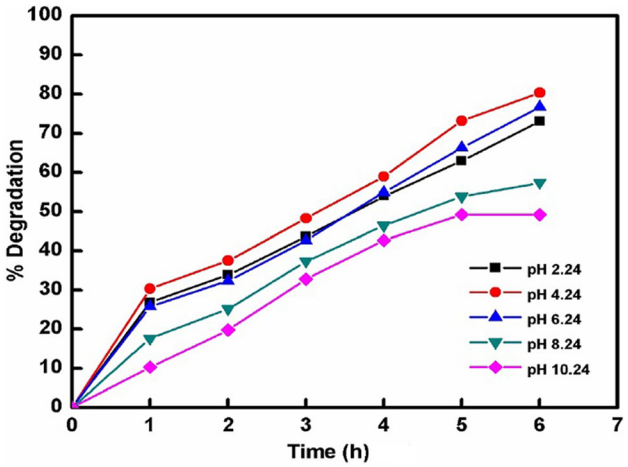


**Figure 7.** Absorbance spectra for 50 ppm MR at 4.24 pH degraded by 0.014 g of $MoS_2$ as catalyst in 6 h.

hydroxyl radical attack. It can be explained on the basis of zero-point charge and acid–base property of the metal oxide surface [46]. Since acid–base properties of the metal oxide surfaces exhibit major effect of pH on the photocatalysis, the adsorption of molecules of dye on the $MoS_2$ surface is highly influenced by variation in pH. When water molecules are adsorbed at the surface of $MoS_2$, it leads to the breakage of OH– charge group from $MoS_2$ and replaced by chemically equivalent metal hydroxyl groups (M–OH). This leads to the formation of hydroxyl radicals from hydroxide ions and positive holes. It is considered that the positive holes play a major role as oxidation agent at low pH, whereas at higher level of pH the hydroxyl radicals act as the predominant agent for oxidation [47, 48]. It is stated that hydroxyl radicals could be easily generated in alkaline solution, as $MoS_2$ surface contains more hydroxide ions which in turn enhances the efficiency of the process of photocatalysis. However, due to Coulomb's repulsion, hydroxide anions and negative charge on the surface of the catalyst inhibit the formation of hydroxyl radicals. Thus, the hydroxyl radicals do not react with the dye molecules easily. As a result, adsorption of dye on the surface of photocatalyst is greatly reduced [49–51]. However at low pH, electrons in the conduction band play an active role in the degradation of dyes by reductive cleavage of azo bonds. This reduction by electrons take place due to electrostatic interactions between the dye anions and positively charged surface of the catalyst, which leads to strong adsorption of dye on the catalyst surface. At lower pH, tendency of agglomeration of catalyst particles occur, which reduces the availability of the surface area for adsorption of dye. Another reason attributed to the higher degradation rate in acidic condition goes to the formation of strong surface complex bonds, which enhances the efficiency of the electron-transfer process. But this effect is less pronounced in neutral or basic pH conditions [52]. All these reasons attribute to improved photocatalysis of MR in acidic conditions, which however decreases when pH is increased. Similar trend was observed by many groups [53, 54].

From above results, figure 7 exhibits absorbance spectra of MR for an optimum dosage of 0.014 g of $MoS_2$ catalyst with 4.24 pH and 50 ppm of dye concentration. It is concluded that at this concentration of catalyst, dye concentration and pH, enhanced degradation (80.35%) of the MR with 0.4278 $h^{-1}$ rate constant is observed. Photocatalytic degradation behaviour of MR under irradiation by visible light might have proceeded via two possible processes: photocatalytic oxidation and photo-sensitized oxidation as discussed by our group earlier [39]. In the former mechanism, when $MoS_2$ NSs are irradiated by visible light, the photo-excitation of the semiconductor leads to the generation of electron–hole pair ($e^-_{CB}$ from the conduction band and $h^+_{VB}$ from the valence band) on the surface of the catalyst. On the other hand in photo-sensitizing mechanism, instead of the catalyst, the adsorbed dye itself gets excited to singlet or triplet states under the visible-light irradiation and injects electron to the conduction band of $MoS_2$ NSs. Both the mechanisms of photo-oxidation and photo-sensitization goes side by side. It is not possible to explain which of the mechanism is superior but it is established that photo-sensitizing mechanism improves the efficiency of photo-oxidation degradation of dyes and makes the process more feasible.

## 5. Conclusions

In summary, the $MoS_2$ NSs have been synthesized with high yield successfully by a simple, cost-effective hydrothermal method. It has been further characterized to exhibit its

application as a photocatalyst for the removal of azo dye (MR). From the X-ray diffraction results, we confirm the formation of as-synthesized $MoS_2$ NSs. However, the spherical morphology of $MoS_2$ NSs was well explained by the transmission electron microscope results. Raman spectra ensures the formation of 5–6 layers of these $MoS_2$ NSs. UV–visible absorbance spectra confirm the optical properties of $MoS_2$ NSs in the region of UV–visible light spectrum. Further, we exhibit a detailed discussion on the effect of various factors on the degradation of the dye, like catalyst dosage ($MoS_2$ NSs), concentration of pollutant (MR) and pH variation of the pollutant dye. A maximum of 80.35% degradation with 0.4278 $h^{-1}$ rate constant for 50 ppm MR at 4.24 pH appeared at 6 h with the optimized 14 mg dosage of $MoS_2$ NSs. The photocatalytic degradation of MR is attributed to the presence of chromophoric sites.

## References


[1] Khataee A R and Kasiri M B 2010 *J. Mol. Catal. A Chem.* **328** 8
[2] Ruiz A M, Sakai G, Cornet A, Shimanoe K, Morante J R and Yamazoe N 2004 *Sens. Actuators B Chem.* **103** 312
[3] Neppolian B, Choi H C, Sakthivel S, Arabindoo B and Murugesan V 2002 *Chemosphere* **46** 1173
[4] Saquib M and Muneer M 2003 *Dye Pigment* **56** 37
[5] Galindo C, Jacques P and Kalt A 2001 *Chemosphere* **45** 997
[6] Das S, Kamat P V, Padmaja S, Au V and Madison S A 1999 *J. Chem. Soc. Perkin Trans.* **2** 1219
[7] Yang Y, Wyatt D T and Bahorsky M 1998 *Text. Chem. Color* **30** 27
[8] Guillard C, Lachheb H, Houas A, Ksibi M, Elaloui E and Herrmann J M 2003 *J. Photochem. Photobiol. A Chem.* **158** 27
[9] Zhu S and Wang D 2017 *Adv. Energy Mater.* **7** 1700841
[10] Sharma M, Mohapatra P K and Bahadur D 2017 *Front Mater. Sci.* **11** 366
[11] Malligavathy M, Iyyapushpam S, Nishanthi S T and Padiyan D P 2018 *Pramana - J. Phys.* **90** 1
[12] Sumesh C K and Parekh K 2019 *Pramana - J. Phys.* **92** 87
[13] Rani A, Singh K, Patel A S, Chakraborti A, Kumar S, Ghosh K *et al* 2020 *Chem. Phys. Lett.* **738** 136874
[14] Rani A, Singh K, Patel A S, Chakraborti A and Sharma P 2021 *J. Mater. Sci: Electron.* **32** 6168
[15] Bisaria K, Sinha S, Singh R and Iqbal H M N 2021 *Chemosphere* **284** 131263
[16] Xu C, Ravi Anusuyadevi P, Aymonier C, Luque R and Marre S 2019 *Chem. Soc. Rev.* **48** 3868
[17] Altintas Yildirim O, Arslan H and Sönmezoğlu S 2016 *Appl. Surf. Sci.* **390** 111
[18] Vattikuti S V P and Byon C 2016 *Superlattices Microstruct.* **100** 514
[19] Tab A, Bellal B, Belabed C, Dahmane M and Trari M 2020 *Optik (Stuttg)* **214** 164858
[20] Bumajdad A, Madkour M, Abdel-Moneam Y and El-Kemary M 2014 *J. Mater. Sci.* **49** 1743
[21] Pan D, Jiao J, Li Z, Guo Y, Feng C, Liu Y *et al* 2015 *ACS Sustain. Chem. Eng.* **3** 2405
[22] Emeline A V, Kuznetsov V N, Rybchuk V K and Serpone N 2008 *Int. J. Photoenergy* **2008** 258394
[23] Wang J A, Limas-Ballesteros R, Lopez T, Moreno A, Gomez R, Novaro O *et al* 2001 *J. Phys. Chem. B* **105** 9692
[24] Sacco O, Stoller M, Vaiano V, Ciambelli P, Chianese A and Sannino D 2012 *Int. J. Photoenergy* **2012** 626759
[25] Gaim Y T, Tesfamariam G M, Nigussie G Y and Ashebir M E 2019 *J. Compos. Sci.* **3** 93
[26] Meshram S P, Adhyapak P V, Pardeshi S K, Mulla I S and Amalnerkar D P 2017 *Powder Technol.* **318** 120
[27] Mishra A K, Lakshmi K V and Huang L 2015 *Sci. Rep.* **5** 1
[28] Quinn M D J, Ho N H and Notley S M 2013 *ACS Appl. Mater. Interfaces* **5** 12751
[29] Johari P and Shenoy V B 2012 *ACS Nano* **6** 5449
[30] Prabukumar C, Mohamed Jaffer Sadiq M, Krishna Bhat D and Udaya Bhat K 2019 *Mater Res. Express* **6** 085526
[31] Zhang W, Xiao X, Zheng L and Wan C 2015 *Can. J. Chem. Eng.* **93** 1594
[32] Chen B, Meng Y, Sha J, Zhong C, Hu W and Zhao N 2018 *Nanoscale* **10** 34
[33] Benavente E, Durán F, Sotomayor-Torres C and González G 2018 *J. Phys. Chem. Solids* **113** 119
[34] Luo L, Shi M, Zhao S, Tan W, Lin X, Wang H *et al* 2019 *J. Saudi Chem. Soc.* **23** 762
[35] Ntakadzeni M, Anku W W, Kumar N, Govender P P and Reddy L 2019 *Bull. Chem. React. Eng. Catal.* **14** 142
[36] Ho W, Yu J C, Lin J, Yu J and Li P 2004 *Langmuir* **20** 5865
[37] Reza K M, Kurny A and Gulshan F 2017 *Appl. Water Sci.* **7** 1569
[38] Azeez F, Al-Hetlani E, Arafa M, Abdelmonem Y, Nazeer A A, Amin M O *et al* 2018 *Sci. Rep.* **8** 7104
[39] Rani A, Singh K and Sharma P 2022 *Bull. Mater. Sci.* **45** 63
[40] Tian Y, He Y and Zhu Y 2004 *Mater. Chem. Phys.* **87** 87
[41] Lee C, Yan H, Brus L E, Heinz T F, Hone J and Ryu S 2010 *ACS Nano* **4** 2695
[42] Daneshvar N, Salari D and Khataee A R 2003 *J. Photochem. Photobiol. A Chem.* **157** 111
[43] Reutergardh L B and Iangphasuk M 1997 *Chemosphere* **35** 585
[44] Poulios I and Aetopoulou I 1999 *Environ. Technol.* **20** 479
[45] Kansal S K, Kaur N and Singh S 2009 *Nanoscale Res. Lett.* **4** 709
[46] Konstantinou I K and Albanis T A 2004 *Appl. Catal. B Environ.* **49** 1
[47] Poulios I and Tsachpinis I 1999 *J. Chem. Technol. Biotechnol.* **74** 349
[48] Tang W Z and Huang C P 1995 *Water Res.* **29** 745
[49] Tunesi S and Anderson M 1991 *J. Phys. Chem.* **95** 3399
[50] Galindo C, Jacques P and Kalt A 2000 *J. Photochem. Photobiol. A Chem.* **130** 35
[51] Stylidi M, Kondarides D I and Verykios X E 2003 *Appl. Catal. B Environ.* **40** 271
[52] Lachheb H, Puzenat E, Houas A, Ksibi M, Elaloui E, Guillard C *et al* 2002 *Appl. Catal. B Environ.* **39** 75
[53] Bandara J, Mielczarski J A and Kiwi J 1999 *Langmuir* **15** 7680
[54] Tanaka K, Padermpole K and Hisanaga T 2000 *Water Res.* **34** 327